A Portable X-Band Front-End Test Package for Beam-Waveguide Antenna Performance Evaluation Part II: Tests on the Antenna

T. Y. Otoshi, S. R. Stewart, and M. M. Franco
Ground Antennas and Facilities Engineering Section

Part I described an X-band (8.45 GHz) test package for testing the new 34-m beam-waveguide antenna at Goldstone. In addition, results were given for the test package in an "on-the-ground" configuration. This article gives results for the test package in an "on-the-antenna" configuration. Included are X-band zenith noise-temperature values and tipping-curve data obtained at the Cassegrain focal point F1 as well as at the pedestal room focal point F3. Subreflector Z-defocus test results for both F1 and F3 are also presented. The X-band test package operated well in all of the different test configurations and exceeded expected performance.

I. Introduction

As described in Part I [1], a test package has been developed to test the new 34-m beam-waveguide (BWG) antenna at X-band (8.45 GHz). The portable test package can be transported to different focal point locations of the BWG system. The degradations caused by the BWG mirror systems are determined by differencing the measured parameters at the different focal points (Fig. 1).

Part I gave the results of noise-temperature measurements for the X-band test package on the ground at 8.45 GHz. This article presents the results of zenith operating system noise-temperature measurements as well as results from tipping-curve and subreflector tests on the new BWG antenna at the Cassegrain focal point F1 and at the pedestal room focal point F3.

Noise-temperature symbols are used in many of the tables in this article. For the reader's convenience, the symbols are defined in Table 1.

II. Installations

Figure 2 shows the X-band 29-dBi horn test package installed on the antenna at F1. A removable wooden floor (not shown) about 12 inches below the test package and a ladder (shown in Fig. 2) are parts of a temporary installation. This installation facilitates ease of connecting cables and servicing the test package. The structure shown supporting the X-band test package is a universal mount that allows any of the three 29-dBi horn configuration test packages (X-band, 8.45 GHz; Ku-band, 12 GHz; and Ka-band, 32 GHz) to be interchanged and installed. A tape

measure showed that the desired and actual horn phase center locations agreed to within 1/4 to 1/8 in., with measurements accurate to ±1/16 in. Any error of up to 2 or 3 inches in the phase center location in the Z direction can be compensated for by readjustment of the subreflector.

After completion of noise-temperature and antenna-efficiency measurements at F1, the X-band test package was removed, reconfigured to a 22-dBi horn configuration and installed at F3 (Fig. 3). The mounting table shown in Fig. 3 is a universal mount that can support any of the test packages (X-, Ku-, or Ka-band) and provides three-axis adjustment of the test package location. Adjustments of ±3 in. can be made along three orthogonal axes (i.e, the vertical direction, the radial direction towards and away from the hub center, and the other transverse direction).

III. Test Results

A. Preliminary Diagnostics Work

When the X-band test package was first installed at F1 and the new BWG antenna was tested, the zenith noise temperature was about 28 K as compared to an expected value of about 26 K. Various tests were run to isolate contributors to the high noise-temperature values. Six contributors were found and are listed in Table 2. With the exception of noise contributed from the open hub area below the feed horn, all noise contributions from various sources were minimized or eliminated by covering openings with perforated sheets or aluminum tape.

B. Zenith Noise-Temperature Measurements

Figures 4(a) and (b) show typical mini-cal [1] plots with the 29-dBi horn test package mounted at F1 and with all of the contributors of Table 2 eliminated except item 6. Figure 5 shows a mini-cal plot of the operating system temperature when the test package was mounted at F3. For these plots, corrections were made for gain changes but no corrections were made for nonlinearity, which was typically less than 1 percent. Since the uncertainty of the linearity corrections is itself about ±1 percent, the small linearity corrections, if made, would not significantly enhance the quality of the system noise-temperature data shown on these particular plots.

A summary of results of X-band zenith operating system noise temperatures for the ground and the F1 and F3 locations is given in Table 3. The value shown in the table for each test configuration is the grand average of the average operating system temperature determined for the individual observing periods. Observations were made over a 7-month period. Each grand average value shown in Table 3 is estimated to have an uncertainty of ±0.5 K (one standard deviation).

Although some F2 measurements were performed for diagnostic purposes, they are not included in Table 3. The F2 measurements were questionable due to uncertainties as to whether or not a low-noise diode signal from the noise box (Fig. 6) had been left on during the F2 testing.

When the test package is on the ground, the general expression for the operating system temperature is

$$T_{op} = T'_{cb}/(L_{atm}L_{wg}) + T_{atm}/L_{wg} + T_{wg} + T_{hemt} + T_{fup} \quad (1)$$

Under standard conditions at 8.45 GHz, the component values are T'_{cb} = 2.5 K, T_{atm} = 2.17 K, T_{wg} = 4.69 K, T_{hemt} = 13 K, T_{fup} = 0.4 K, L_{atm} = 1.00814 (corresponding to 0.0352 dB), and L_{wg} = 1.0163 (corresponding to 0.07 dB).

Substitutions of the values into Eq. (1) result in a predicted T_{op} of 22.7 K, which agrees with the measured ground value of 22.7 K shown in Table 3.

Differential noise temperatures for the various configurations are shown in Table 4. The F1-minus-ground-configuration data have a value of 3.2 K, which is due to subreflector scattering, tripod scattering, leakage through the main reflector surface, and main reflector spillover. This value can be compared to an F1-minus-ground-configuration value of 3.8 K for X-band reported for the DSS 15 34-m Cassegrain antenna.[1] The F3-minus-F1-configuration data noise-temperature values provide a measure of the degradation caused by the six mirrors. A slight increase of 0.6 K in the 8.45-GHz noise temperature occurred after the ellipsoid and other five mirrors were realigned for purposes of improving the F3 BWG antenna performance at 32 GHz.

Table 5 is a worksheet showing how the final values summarized in Table 3 were derived. Shown are the observation periods, the measured operating system noise-temperature values, weather information, and normalized values after corrections were made for weather and waveguide physical temperatures. In Table 5, the normalized T_{op} is computed from

[1] A. Freiley, *DSS 15 System Noise Temperature*, JPL Interoffice Memorandum (internal document), Jet Propulsion Laboratory, Pasadena, California, July 15, 1990.

$$T_{op,n} = T_{op} + (T'_{cb}/L_{wg})(1/L_{atm,s} - 1/L_{atm}) + (1/L_{wg})(T_{atm,s} - T_{atm}) + (T_{wg,s} - T_{wg}) \quad (2)$$

where T_{op}, T_{atm}, T_{wg}, and L_{atm} are, respectively, the average measured T_{op} and computed T_{atm}, T_{wg}, and L_{atm} values given in Table 5.

Values for standard DSS 13 atmospheric conditions at 8.45 GHz per DSN Document 810-5[2] are

$T_{atm,s}$ = 2.17 K

$L_{atm,s}$ = 1.00814 (corresponding to 0.0352 dB)

Other X-band (8.45 GHz) values used for Eq. (2) are

T'_{cb} = 2.5 K

L_{wg} = 1.0163 (corresponding to 0.07 dB)

$T_{wg,s}$ = 4.69 K for the above L_{wg} and a standard physical waveguide temperature of 20 deg C

At X-band and higher microwave frequencies, weather changes can cause significant variations of atmospheric noise contributions to operating system noise temperatures. As may be seen in Table 5, the applications of weather corrections enabled significant improvements to be made in the comparisons of operating noise temperatures for the different test configurations even when the measurements were performed on different days (months) of the different test configurations. Figure 7 reveals the sensitivity of DSS 13 X-band atmospheric noise contributions as functions of typical weather parameters during a calendar year. It is of interest to note that, at X-band, different weather conditions during the year at DSS 13 can cause the atmospheric noise temperatures to vary between 1.9 K and 4.2 K. The peak-to-peak variation of 2.3 K for X-band (8.45 GHz) is small compared to a peak-to-peak variation of 27 K that was computed for Ka-band (32 GHz) for the same weather limits shown in Fig. 7.

A computer program, SDSATM7M.BAS,[3] was used to derive values for Fig. 7. In this program the Earth's atmosphere is assumed to be 30 km high and is divided up into 300 layers, each of which is 0.1 km thick. The input data consists of the height of DSS 13 above sea level, barometric pressure, ground-level air temperature, and ground-level relative humidity. From the input data, the average pressure, water vapor, and oxygen content are determined for each layer. In Method 1 of the program, a constant mean physical temperature of 265 K is assumed for each layer for the oxygen noise contribution. For the water vapor, every layer is assumed to be at a constant physical temperature that is 10 K lower than the measured ground-level physical temperature. The noise temperature is computed for each layer and then integrated to arrive at the total atmospheric noise temperature. A more rigorous Method 2 by Otoshi was incorporated into the program as an option to take into account the temperature gradient of water vapor and oxygen content in each layer. Comparisons of the results from the two methods revealed that Method 1, used for the results described in this article, is sufficiently accurate for making corrections for atmospheric noise temperature changes due to weather. It should be pointed out that Method 1 is also being used for making weather corrections to the BWG antenna efficiency measurement data.[4]

C. Tipping Curves

Tipping curve tests were performed at F1 and F3 at various azimuth angles for the test package. A few of the tipping curves are shown in Fig. 8. On a clear day, the tipping curves should be independent of azimuth angles except at elevation angles approaching those that correspond to the ground profile. A horizon profile map shows that the DSS 13 ground profile elevation angle is less than about 1 deg for 50- and 126-deg azimuth angles, but is about 7 deg at the 315-deg azimuth angle.

Due to the high levels of wide-angle side lobes on previous large Deep Space Network (DSN) antennas, it has not been possible to derive the atmospheric noise contributions from the measured operating system temperature values only at zenith and the 30-deg elevation angle. The general equation for extracting the zenith atmospheric noise temperature from tipping-curve data is derived as

$$T_{atmz} = L_{ant}[T_{op}(\theta_{el}) - T_{op}(90)]/[1/\sin(\theta_{el}) - 1] + T'_{cb}(1 - 1/L_{atmz}) \quad (3)$$

where

θ_{el} = the elevation angle, deg

$T_{op}(\theta_{el})$ = the operating system temperature measured at θ_{el}, K

[2] *Deep Space Network Flight Project Interface Design Handbook*, 810-5, rev. D., vol. I, module TCI-30 (internal document), Jet Propulsion Laboratory, Pasadena, California, June 1, 1990.

[3] Courtesy of S. Slobin of the Jet Propulsion Laboratory, Pasadena, California. The SDSATM7M.BAS program is a modified version of SDSATM4.BAS, but gives the same answers.

[4] S. Slobin, private communication, Jet Propulsion Laboratory, Pasadena, California, November 1990.

$T_{op}(90)$ = the operating system temperature measured at $\theta_{el} = 90$ deg or at zenith, K

L_{atmz} = the loss factor for the zenith atmosphere. An estimate of this value can be made by using the loss factor for a standard atmosphere, or a better estimate can be obtained from use of the SDSATM7M.BAS program for the actual weather conditions during the measurement.

T'_{cb} = the effective contribution to T_{op} from the cosmic background, K

L_{ant} = the loss factor from the antenna aperture to the input to the HEMT, K

For the special case of $\theta_{el} = 30$ deg, Eq. (3) becomes

$$T_{atmz} = L_{ant}[T_{op}(30) - T_{op}(90)] + T'_{cb}(1 - 1/L_{atmz}) \quad (4)$$

In practice, the factor L_{ant} is often set equal to 1.0 and the last term in Eq. (4) is often completely ignored. At 8.45 GHz and under standard atmospheric conditions, the last term contributes only 0.02 K. The values used in Eq. (4) to obtain the results in Table 6 were $T'_{cb} = 2.5$ K and $L_{ant} = L_{wg} = 1.0163$ (corresponding to 0.070 dB). For simplicity, the antenna reflector surface and BWG resistive losses were not included in the L_{ant} value.

Table 6 shows a comparison of the measured T_{atm} as obtained through the use of Eq. (4) and computed T_{atm} as obtained through the SDSATM7M program, which is based on the weather data shown. As seen in Table 6, the difference between measured and computed atmospheric noise temperatures is only ±0.2 K at X-band for this antenna. The low amount of scattering from the slim tripod legs on the BWG antenna provides a possible explanation for this good agreement.

D. Subreflector Tests

Figure 9 shows a subreflector defocus curve obtained at F1 at an average elevation angle of 51 deg while tracking radio source 3C274. At the time tests were being done at F1, a good test procedure for obtaining subreflector defocus data with a radio source had not yet been fully developed. Calibrated and annotated strip-chart recordings were used to obtain required data. Hence, the F1 subreflector defocus data are estimated to be accurate only down to the −13-dB level. Also shown in Fig. 9 is a predicted Z-defocus curve that is based on a mechanical structural model by R. Levy and another curve based on a GTD/Jacobi–Bessel antenna program by P. Cramer. The Cramer calculations were done for a rigging angle of 45 deg and, therefore, do not include any gravity effects.[5] It can be seen in Fig. 9 that the agreements between predicts from the two theoretical models and the experimental data are quite good down to about −12 dB.

For verification of the performance of the antenna optics at F3, a subreflector Z-defocus test was performed in the region of the 45-deg elevation angle. In contrast to the strip chart method used for F1 tests, for F3 tests the operating system temperature data for each subreflector offset position were averaged by the computer and sent to both a line printer and a disk file. Figure 10 shows a comparison of predicts for F1 and experimental results at F3. It should be pointed out that even though Cramer's predicts were made for F1 and the experimental results are for F3, there is good agreement between theory and experiment. Note also that good agreement is still obtained between Cramer's predicts and experimental results at defocus positions in the side-lobe regions of the subreflector defocus curve. For a properly designed and aligned BWG mirror system, the subreflector defocus gain curves at F3 should be nearly identical to those at F1. Therefore, a Z-defocus subreflector test at F3 provides a good method for verifying the integrity of the BWG system.

A Z-defocus subreflector test is also useful for revealing whether multipath signals exist within a large antenna system [3,4]. Scrutiny of the subreflector defocus data near the peak of the main beam (Fig. 11) indicates there are no unusual humps, as were found on a 64-m S-band (2295 MHz) Cassegrain antenna [3]. The absence of humps and ripples on the main beam defocus curve shown in Fig. 11 indicates that the magnitudes of any multipath signals within the BWG system are probably small.

Unlike Y-defocus tests, when Z-defocus tests are performed, new sets of boresight readings do not have to be obtained at each new subreflector setting. However, a sufficient number of off-boresight and on-source readings need to be obtained to enable corrections to be made for potential receiver gain changes. A Z-defocus test can be performed rather quickly (1.5 hr). If too much time is taken to perform a subreflector test, the antenna characteristics (which are functions of elevation angle) will change sufficiently as to invalidate the test at a desired average elevation angle.

In order to obtain accurate subreflector defocus data below the 13-dB level (Figs. 9 and 10) while tracking a

[5] P. Cramer, *Calculated DSS-13 Subreflector Z-axis Focus Curves, Feed at F1*, JPL Interoffice Memorandum 3328-90-0355 (internal document), Jet Propulsion Laboratory, Pasadena, California, September 20, 1990.

10 K source, the radiometer needs to provide resolutions and accuracies better than 0.2 K. In addition, the antenna-pointing model should be sufficiently good so as to allow blind pointing and remain on the peak of the source to within ±4 mdeg.

E. Overall Performance

The overall performance of the X-band test package is summarized in Table 7. The performance data are based on observed test data in a worst-case field environment as well as on error analysis equations given in [5]. Examination of Table 7 reveals that the X-band test package performance was excellent in terms of resolution, gain stability, and linearity.

The test package was subjected not only to mechanical stresses during radio source tracking at various elevation angles at F1, but also to ambient temperatures ranging from 0 to 40 deg C and transportation to and from the ground, F1, and F3 several times. Test data in Table 3 show that the long-term stability and repeatability of data for the various test configurations were very good.

IV. Conclusions

The goal of obtaining accurate noise-temperature values with the test package at the various focal points has been achieved. The X-band test package has operated well in all of the different test configurations and performed better than expected in terms of short- and long-term gain stability. To the authors' knowledge, the results presented in this article demonstrate the first known experimental method for determining the degradations caused by the BWG system of any large antenna.

Acknowledgments

Numerous persons have contributed to the acquisition of high-quality data. Many who contributed to the test package development have been previously acknowledged in Part I. Those who contributed to obtaining the results reported in Part II are acknowledged here. The Goldstone crew, supervised by J. Carpenter and J. May, installed the test package at F1 and F3 and their efforts are gratefully acknowledged. J. Garnica and G. Bury of DSS 13 assisted in obtaining the F1 noise-temperature diagnostics data given in Table 2. Scheduling conflicts for F1 and F3 tests were resolved by the Test Coordinator, M. Britcliffe of the Ground Antennas and Facilities Engineering Section. The continual on-site support of DSS 13 personnel and DSS 13 supervisor C. Goodson is gratefully acknowledged. Without the contributions and cooperation of both named and unnamed individuals in various groups throughout the Telecommunications Division and the assistance of Goldstone personnel, this project could not have been brought to a successful conclusion.

References

[1] T. Y. Otoshi, S. R. Stewart, and M. M. Franco, "A Portable X-band Front-End Test Package for Beam-Waveguide Antenna Performance Evaluation—Part I: Design and Ground Tests," *TDA Progress Report 42-103*, vol. July–September 1990, Jet Propulsion Laboratory, Pasadena, California, pp. 135–150, November 15, 1990.

[2] C. T. Stelzried, *The Deep Space Network—Noise Temperature Concepts, Measurements, and Performance*, JPL Publication 82-33, Jet Propulsion Laboratory, Pasadena, California, pp. 2-1–2-3, September 15, 1982.

[3] G. S. Levy, D. A. Bathker, A. C. Ludwig, D. E. Neff, and B. L. Seidel, "Lunar Range Radiation Patterns of a 210-ft Antenna at S-band," *IEEE Transactions on Antennas and Propagation*, vol. AP-15, no. 2, pp. 311–313, March 1967.

[4] T. Y. Otoshi and D. L. Brunn, "Multipath Tests on 64-m Antennas Using the Viking Orbiter-1 and -2 Spacecraft as Far-Field Illuminators," *DSN Progress Report 42-31*, vol. November and December 1975, Jet Propulsion Laboratory, Pasadena, California, pp. 41–49, February 15, 1976.

[5] C. T. Stelzried, "Operating Noise-Temperature Calibrations of Low-Noise Receiving Systems," *Microwave Journal*, vol. 14, no. 6, pp. 41–46 and 48, June 1971.

Table 1. Symbols and abbreviations

Symbol	Definition
T_{cb}'	Effective noise temperature contribution to T_{op} from the cosmic background radiation, K. This value is a function of frequency and will differ from the actual cosmic background noise temperature of 2.7 K. (See [2] and Note at the end of this table.)
T_{cb}	Cosmic background radiation noise temperature (nominally 2.7 K)
h	Planck constant
f	Frequency, Hz
k	Boltzmann constant
T_{atm}	Atmospheric noise temperature, K
T_{wg}	Noise temperature due to waveguide loss between the horn aperture and the input flange of the HEMT, K
T_{hemt}	Effective noise temperature of the HEMT as defined at the input flange of the HEMT, K
T_{fup}	Effective noise temperature of the follow-up receiver (downconverter + cables + power meter, etc.) as defined at the input flange of the HEMT, K
T_{op}	Operating system noise temperature as defined at the input flange of the HEMT, K
T_s	Source noise temperature, K
RH	Relative humidity
HEMT	High-electron-mobility transistor
L_{wg}	Loss factor for waveguide between the horn aperture and the input flange of the HEMT, ratio
L_{atm}	Loss factor of the atmosphere, ratio

Note : $T_{cb}' = T_{cb}\left[\frac{x}{\exp(x)-1}\right]$ where $x = \frac{hf}{kT_{cb}}$.

Table 2. Preliminary diagnostic tests at F1: sources of contributions to operating SNT at 8.45 GHz

No.	Contributor description	Noise temperature, K
1	Hoist panels removed	0.4
2	Hatch door open	0.1
3	Open areas at bases of tripod legs	0.2
4	Primary shroud opening for the bypass mode	0.4
5	Openings at the base of bypass shroud on dish surface	0.4
6	Open area below the feed horn for the center pass mode (for tests at F1 only)	0.6

Table 3. Summary of X-band zenith operating system temperatures at DSS 13, from June 10, 1990 to February 2, 1991

Configuration	Observation dates	Grand average[a] T_{op}, K	Peak deviations from grand average, K
Ground	06/10/90, 01/21/91, 01/26/91	22.7	+0.3 −0.3
F1	10/04/90	25.9	—
F3	11/06/90, 11/09/90	34.2	+0.1 −0.2
After mirrors and ellipsoid realigned on December 18, 1990			
F3	01/31/91, 02/02/91	34.8	+0.1 −0.1

[a] See Table 5 for the average T_{op} for each observation period. These values formed the basis for obtaining the grand average for a particular test configuration.

Table 4. Differential zenith operating system temperatures for various test configurations at 8.45 GHz

Configurations differenced[a]	Delta T_{op}, K
F1−Ground	3.2
F3−F1	8.3
After mirrors and ellipsoid realigned on December 18, 1990	
F3−F1	8.9

[a] See Table 3 for ground, F1, and F3 values.

Table 5. X-band (8.45 GHz) measured zenith operating system temperatures corrected for weather and waveguide loss changes

Configuration	Observation period	Average measured T_{op}, K	Average weather during observation	Computed T_{atm}, K	Computed L_{atm}	Physical waveguide temp., deg C	T_{wg}, K	Normalized[a] T_{op}, K
X-band, ground	06/10/90 DOY 161 0800–1200 UT	23.10	891.8 mbar 17.8 deg C 74.4% RH	2.89	1.0108	17.6	4.65	22.4
X-band, ground	01/21/91 DOY 021 1649–1652 UT	22.39	898.2 mbar 4.9 deg C 22.6% RH	2.16	1.0081	8.6	4.51	22.6
X-band, ground	01/26/91 DOY 026 0600–1200 UT	22.73	896.5 mbar 6.5 deg C 36.7% RH	2.22	1.0084	2.2	4.40	23.0
X-band, F1	10/04/90 DOY 277 0800–1200 UT	26.03	900.0 mbar 25.7 deg C 20.4% RH	2.36	1.0088	19.8	4.68	25.9
X-band, F3	11/06/90 DOY 310 0600–1500 UT	33.98	890.0 mbar 8.9 deg C 27.4% RH	2.16	1.0082	17.5	4.65	34.0
X-band, F3	11/09/90 DOY 313 0900–1600 UT	34.45	902.4 mbar 16.0 deg C 29.4% RH	2.32	1.0088	20.7	4.70	34.3
After mirrors and ellipsoid realigned on 91 DOY 018								
X-band, F3	01/31/91 DOY 031 0900–1500 UT	34.63	902.9 mbar 4.7 deg C 13.7% RH	2.11	1.0080	20.7	4.70	34.7
X-band, F3	02/02/91 DOY 033 0730–1330 UT	34.91	899.5 mbar 6.0 deg C 18.8% RH	2.13	1.0081	21.9	4.72	34.9

[a] Normalized T_{op} values were computed through the use of Eq. (2).

Table 6. Measured and computed zenith atmospheric noise temperatures at X-band (8.45 GHz)

Observation period	Average weather	Configuration	Azimuth angle, deg	Computed[a] T_{atm}, K	L_{atmz}	$T_{op}(30) - T_{op}(90)$, K	Measured[b] T_{atm}, K	Delta T_{atm}, K
07/09/90 DOY 190 1950–2050 UT	895.9 mbar 30.9 deg C 20.8% RH	F1	50.9	2.48	1.0092	2.30	2.36	0.12
07/09/90 DOY 190 1950–2050 UT	895.9 mbar 30.9 deg C 20.8% RH	F1	126.5	2.48	1.0092	2.41	2.47	0.01
10/25/90 DOY 298 1638–1706 UT	895.0 mbar 26.0 deg C 13.0% RH	F3	50.0	2.19	1.0083	2.16	2.22	−0.03
01/30/91 1991 DOY 30 2110–2143 UT	902.0 mbar 10.5 deg C 10.2% RH	F3	315.0	2.09	1.0080	2.27	2.33	−0.24

[a] Computed values were obtained from the computer program SDSATM7M.BAS.
[b] Measured value obtained from zenith and 30-deg elevation T_{op} values of the tipping curve, and Eq. (4).

Table 7. X-band test package performance characteristics

Parameter	Performance achieved
Receive polarization	RCP, LCP, or fixed linear
Receive frequencies	8.4–8.5 GHz (determined by fixed local oscillator and IF filter in downconverter)
T_{op} for test package on the ground at DSS 13	< 23 K
Gain stability over 0 to 40 deg C	< 0.3 dB p–p, < 0.05 dB/hr (ovenized heating temperature control)
Delta T_{op} resolution, τ = 1 sec, 100 MHz bandwidth	< 0.02 K
Total calibration nonlinearity error	< 1%
T_s measurement accuracy	$\pm[0.02 + 0.010 \times T_s]$ K for $2 < T_s < 10$ K
Overall T_{op} measurement accuracy, K ($10 < T_{op} < 150$ K)	< 0.4 K p–p

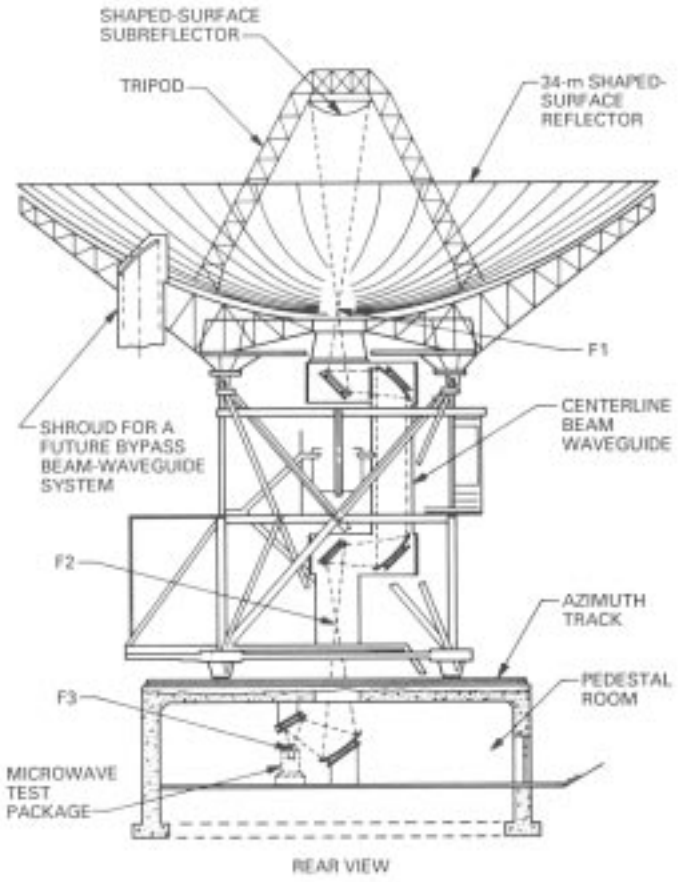

Fig. 1. Beam-waveguide antenna depicting focal points F1, F2, and F3.

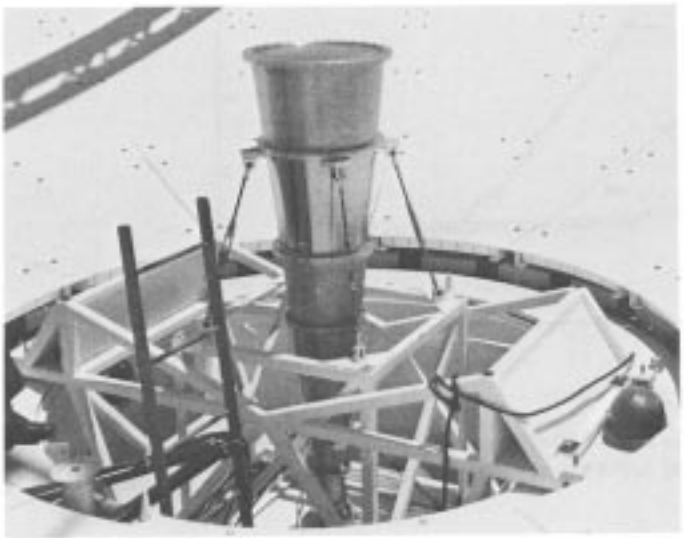

Fig. 2. X-band 29-dBi horn test package and mounting assembly installed at F1.

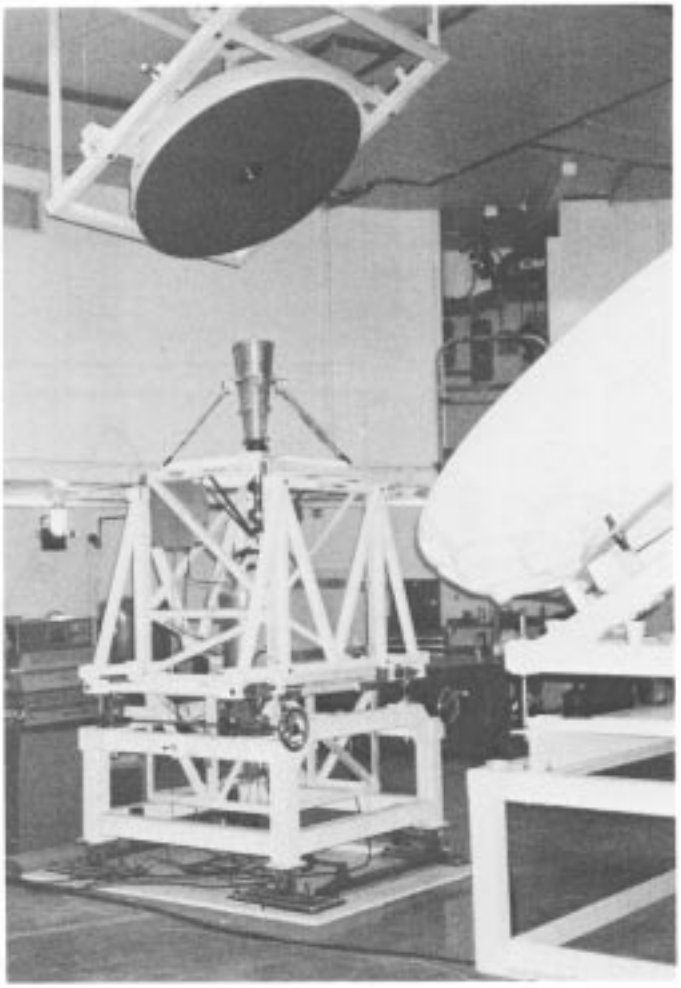

Fig. 3. X-band 22-dBi horn test package and mounting table installed at F3.

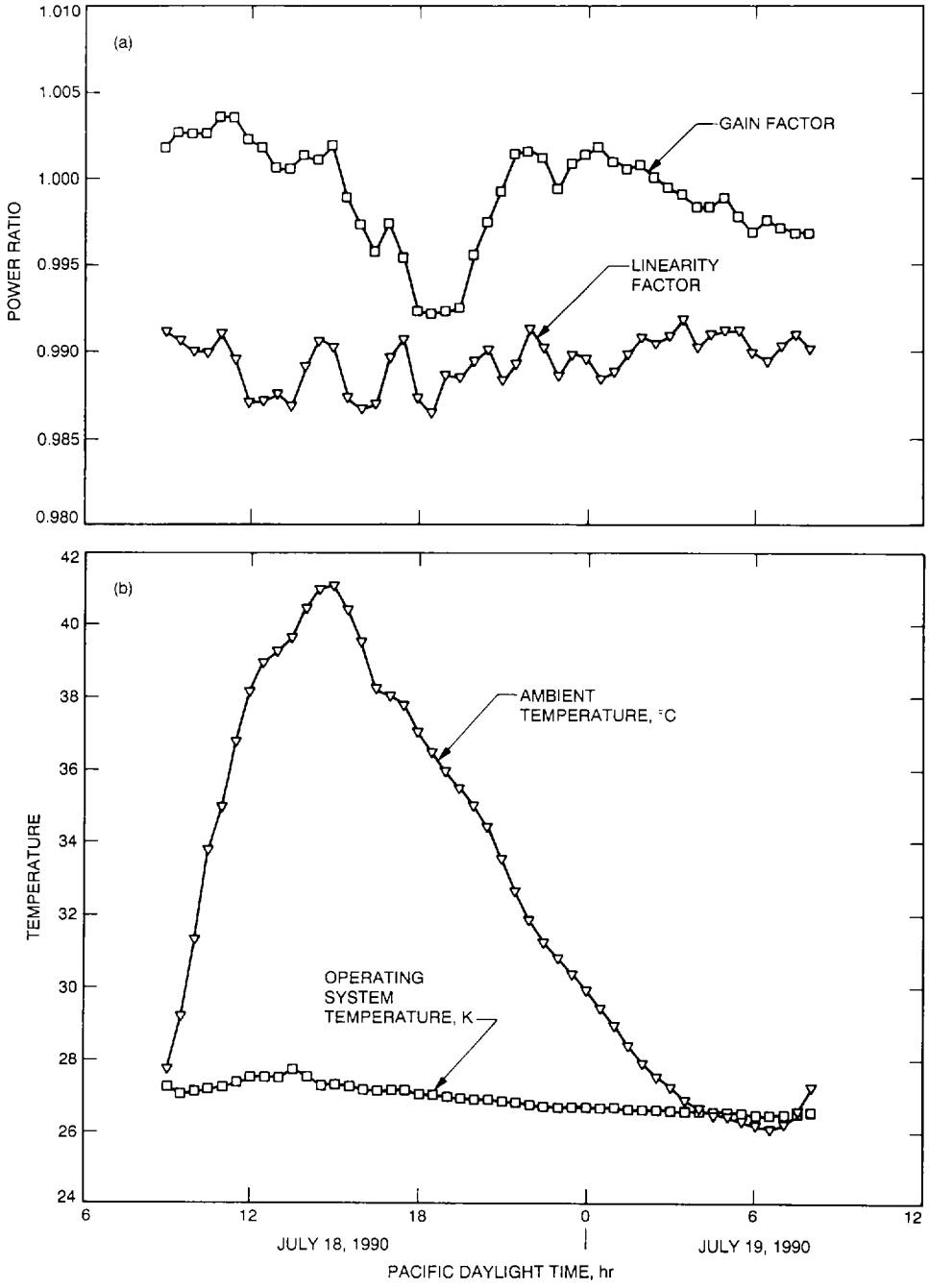

Fig. 4. Mini-cal data taken on July 18, 1990 with the X-band 29-dBi horn test package mounted at F1: (a) gain factor and linearity factor, and (b) operating system noise temperature and ambient temperature.

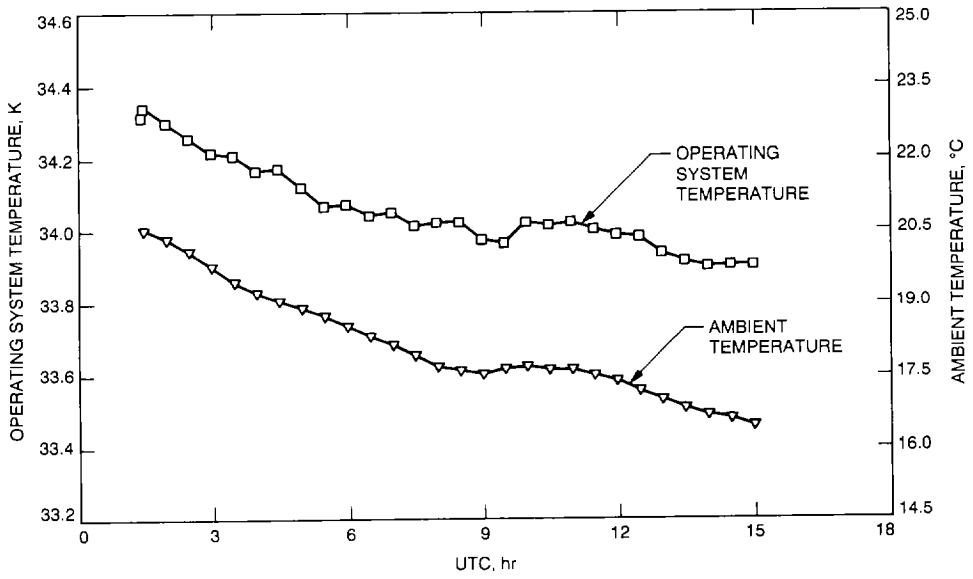

Fig. 5. Operating system noise-temperature mini-cal data taken on November 6, 1990 with the X-band 22-dBi horn test package mounted at F3.

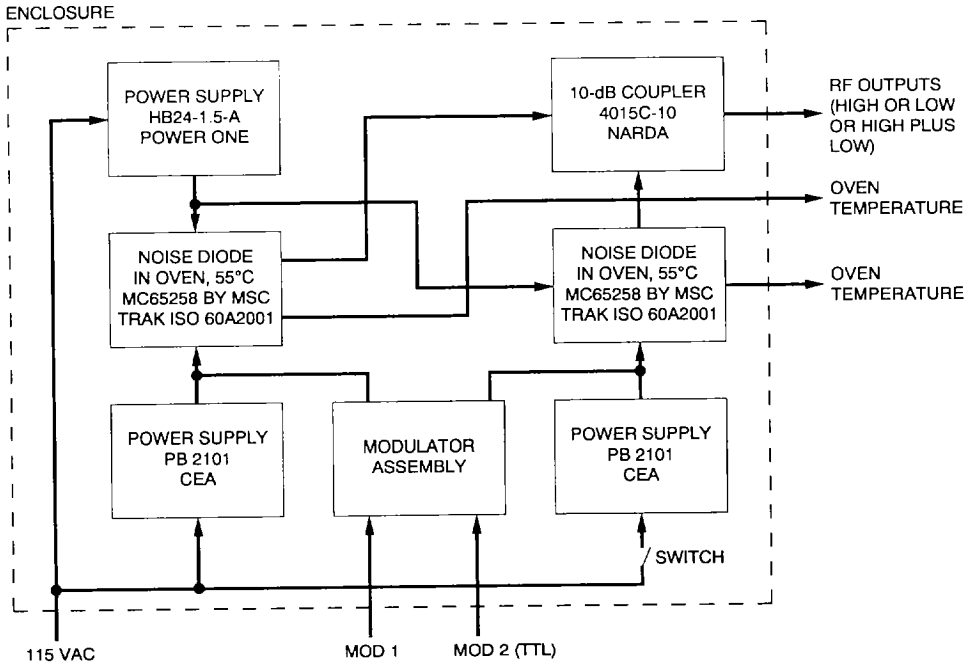

HIGH OUTPUT = $(53 \times 10^{3.5})$ K BEFORE INJECTION INTO THE 35-dB WR125 COUPLER
LOW OUTPUT = $(6.4 \times 10^{3.5})$ K BEFORE INJECTION INTO THE 35-dB WR125 COUPLER

Fig. 6. X-band noise box assembly (mounted inside the X-band test package).

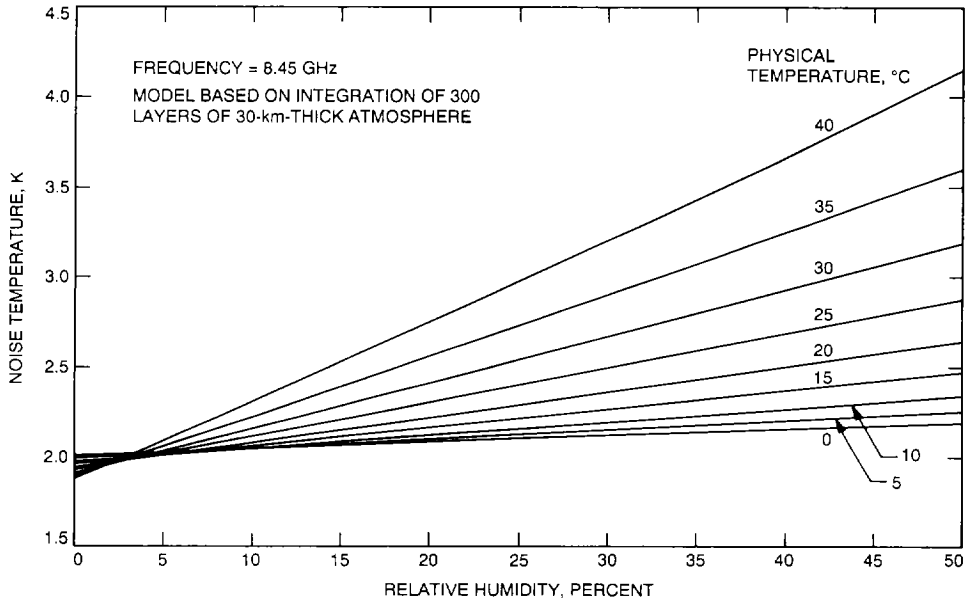

Fig. 7. Theoretical X-band atmospheric noise-temperature contributions versus weather parameters at DSS 13 (courtesy of S. Slobin).

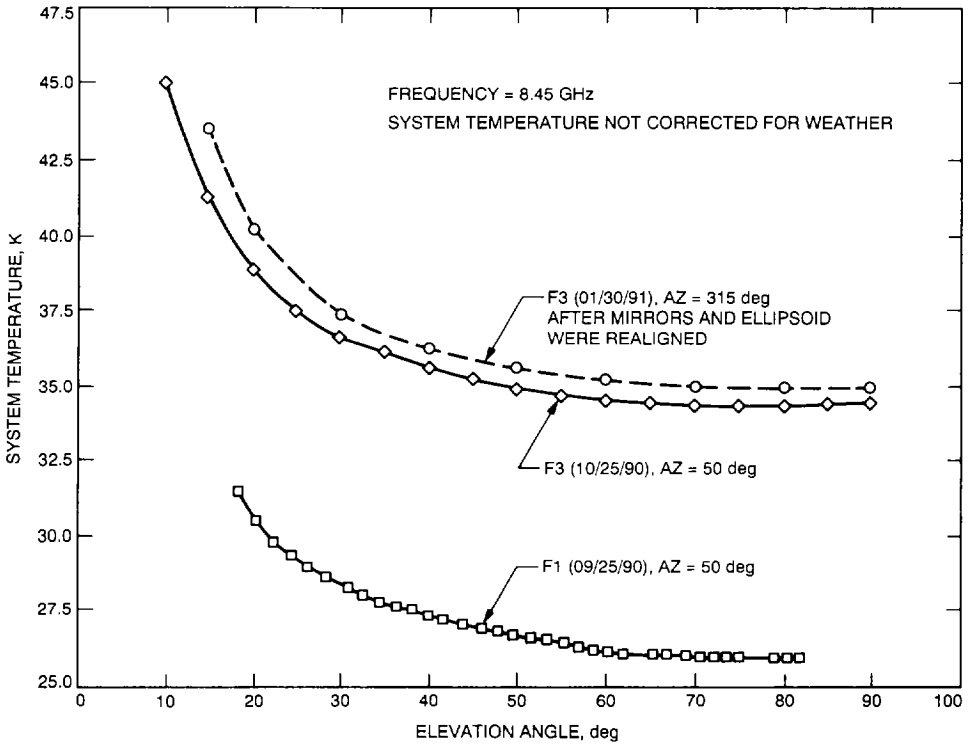

Fig. 8. X-band tipping curves at F1 and F3.

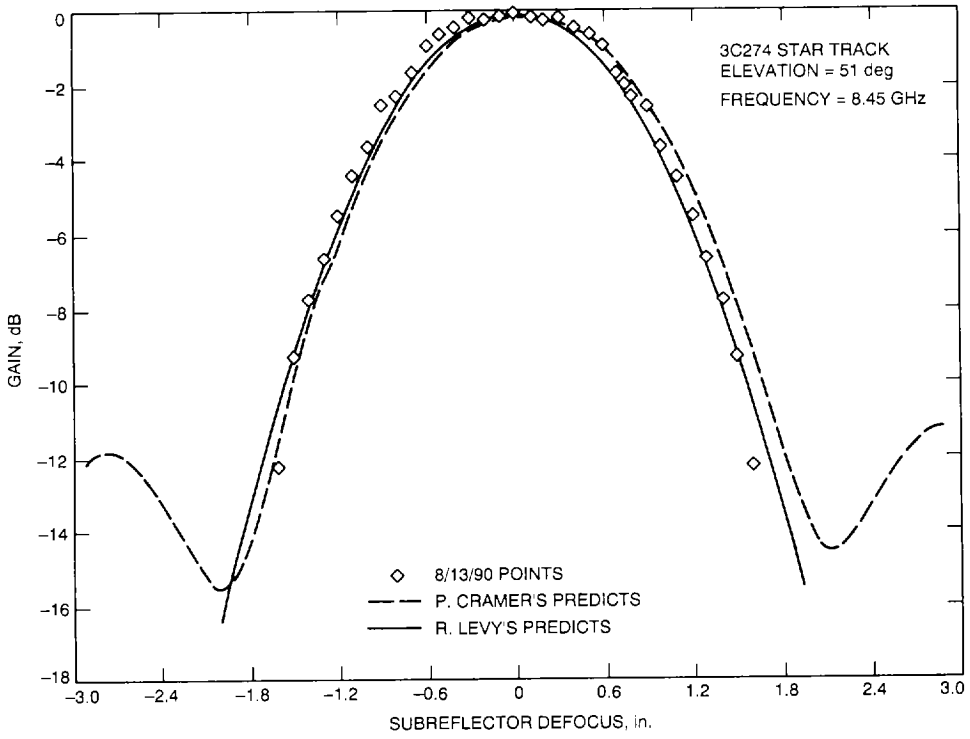

Fig. 9. X-band subreflector *Z*-defocus curve measured at F1.

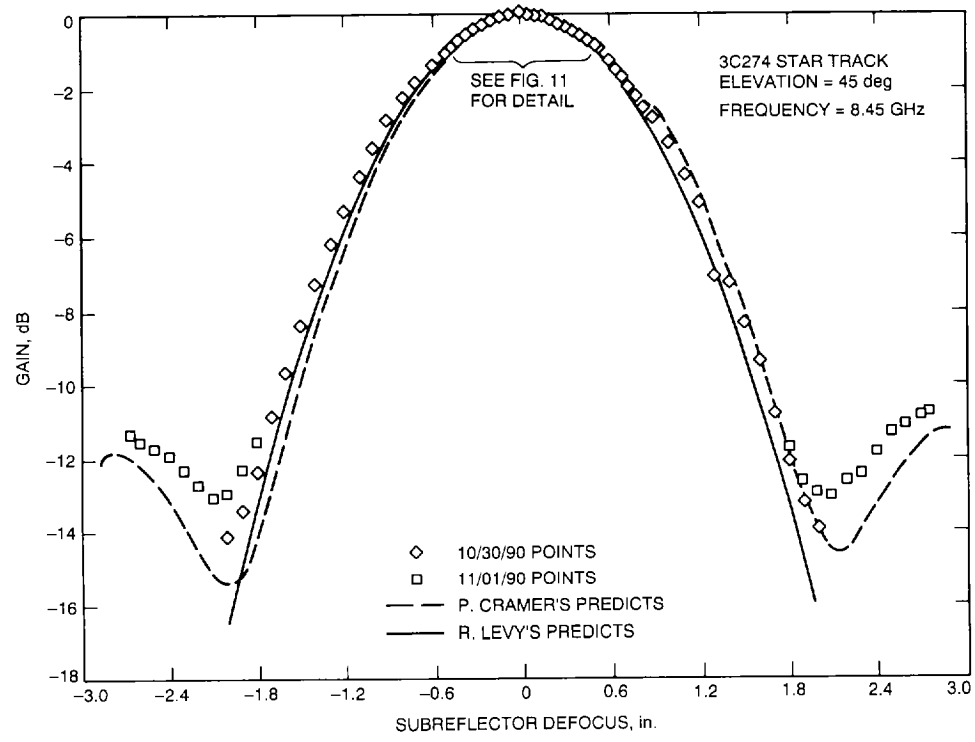

Fig. 10. X-band subreflector *Z*-defocus curve measured at F3.

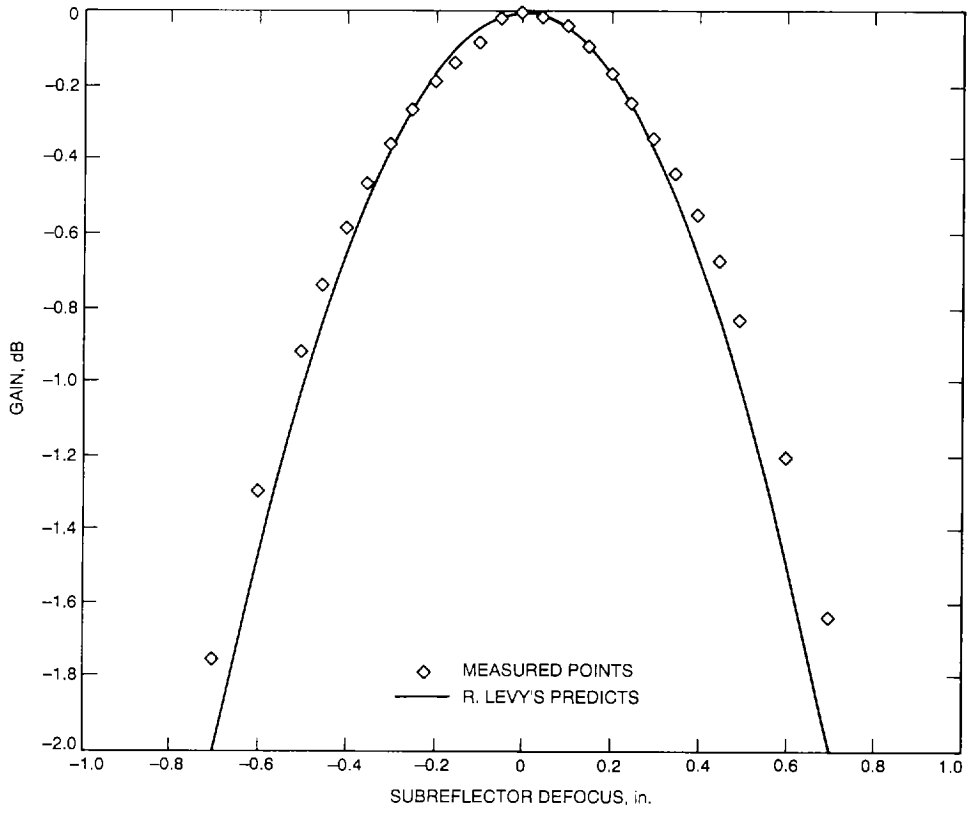

Fig. 11. Expanded detail of main beam of the F3 X-band subreflector defocus curve of Fig. 10.